# Theory of laser-induced free-electron heating and impact ionization in wide-band-gap solids

D. Arnold* and E. Cartier
*IBM Research Division, Thomas J. Watson Research Center, Yorktown Heights, New York 10598*
(Received 10 July 1992)

A microscopic theory for the interaction of intense laser radiation at visible and near-infrared wavelengths with free electrons in a wide-band-gap solid is presented. We calculate the free-electron mediated energy transfer from the laser field to the solid and the electron-multiplication rate due to band-to-band ionization as a function of laser intensity at wavelengths in the range 250 nm $<\lambda<$ 10 $\mu$m, using $SiO_2$ as an example. The formalism is based on a Monte Carlo integration of the Boltzmann transport equation. The electron interaction with the lattice is described in terms of polar and acoustic-phonon scattering. Band-to-band impact ionization is included using an empirical, Keldysh-type impact ionization rate. The interaction of the laser radiation with the free electrons is treated both within the standard classical approximation and quantum mechanically using second-order perturbation theory. We find that the classical approach to the electron-laser field interaction is valid for $\lambda>2$ $\mu$m, while reliable results for short wavelengths, $\lambda<1$ $\mu$m, can only be obtained by using the quantum approach. Second-order perturbation theory is found to fail at long wavelengths, $\lambda>1$ $\mu$m. Both methods are inaccurate for $\lambda\simeq 1$ $\mu$m, yielding only upper and lower bounds for calculated quantities. For $\lambda>2$ $\mu$m the calculated quantities are found to be close to the values obtained in the dc limit, using a dc field equal to the rms value of the ac field. For $\lambda<1$ $\mu$m the electron-multiplication rates decrease dramatically as wavelengths become shorter indicating that multiphoton absorption becomes the dominant mechanism for free-electron generation at visible wavelengths. At all wavelengths the theory predicts efficient free-electron mediated energy transfer from the laser field to the lattice. It is therefore possible to observe significant lattice heating caused by free electrons generated via multiphoton absorption in the prebreakdown regime. These findings are shown to be consistent with recent laser experiments [S. Jones, P. Braunlich, R. Casper, X. Shen, and P. Kelly, Opt. Eng. **28**, 1039 (1989)].

## I. INTRODUCTION

For decades, the breakdown of transparent (wide-band-gap) solids under the action of an intense laser pulse at visible and near-infrared wavelengths has been attributed to electron avalanche formation. Since its first application, the electron avalanche theory has been modified and refined by many authors.[1-5] Most modifications were geared towards a more realistic treatment of the electron-phonon interactions and their energy dependence. All theories, however, have the following basic, simple, and elegant concept in common. Breakdown is assumed to occur above a critical laser intensity (or laser field) because the rate of energy gain from the laser field by a few free electrons exceeds the rate of energy loss to the lattice by phonon scattering. These starting electrons with density $n_0$ rapidly accelerate to kinetic energies larger than the forbidden band gap, undergo impact ionization, and cause free-electron multiplication, leading to an exponential increase of the free-electron density, $n(t)=n_0 2^{\beta(F)t}$, during a laser pulse. Electron densities of the order of $10^{18}$ cm$^{-3}$ are quickly reached, damaging the crystal by excessive Joule heating. The electron-multiplication coefficient $\beta(F)$ itself is a strong function of the laser field, $F$. These theories predict, therefore, that the material will go from ambient temperatures with $n_0$ to high temperatures with $n>10^{18}$ cm$^{-3}$ over a very narrow laser intensity range, with no measurable precursor at lower intensities announcing the impending destructive breakdown. The breakdown intensity (or breakdown field) is thus the only measurable quantity. The detailed nature of the electron-phonon interaction is important only to the extent that it determines the threshold laser intensity for avalanche runaway.

Recent experimental studies in ultrapure alkali halides and in $SiO_2$ on the nonlinear interaction between high-intensity pulsed laser beams and transparent solids have revealed difficulties with the applicability of the electron avalanche theory of laser-induced breakdown at visible and near-infrared wavelengths. A detailed discussion of these experimental results and their implications on breakdown theories can be found in a review by Jones, Braunlich, Casper, Shen, and Kelly.[6] In one experiment, these authors measured the lattice heating by short single laser pulses at a wavelength of 532 nm using photoacoustic detection. It was determined that the lattice temperature increases gradually as a function of laser intensity and that breakdown occurs when the solid reaches a temperature close to its melting temperature. Such a gradual temperature increase with increasing laser intensity cannot be explained in terms of the electron avalanche theories. They concluded that the dominant free-electron generation process is multiphoton absorption rather than impact ionization and that simultaneous free-electron mediated energy transfer from the laser field to the lattice (referred to as "free-electron heating" below) is responsi-

ble for the lattice heating. They obtained a quantitative description of their experiment by combining the theory for free-electron heating developed by Epifanov and coworkers[4,7] with the concept of free-carrier generation by multiphoton absorption. They also confirmed the results of their photoacoustic experiments by measuring the luminescence of the self-trapped excitonic recombination in the prebreakdown regime. The picture, that virtually all lattice heating occurs via nonlinear absorption of laser photons by multiphoton excited free electrons, was further supported by a series of two-color experiments performed on NaCl and $SiO_2$. In these experiments free electrons were generated by a 266-nm pump pulse via three-photon absorption and a delayed 1.064-$\mu$m pulse was used to probe lattice heating in the presence of the generated electron density. The two-color experiment gave the researchers independent control over the starting electron density and the lattice heating. In this manner, they determined that strong lattice heating occurs due to the 1.064-$\mu$m pulse, demonstrating that free-electron heating is an efficient process for energy transfer from the laser field to the lattice.

Theoretically, the validity of the avalanche breakdown model has been investigated by Gorshkov, Epifanov, and Manenkov.[7] They discussed a breakdown model in which both impact ionization and multiphoton absorption are considered as carrier generation processes and showed that a transition from avalanche-induced breakdown to breakdown triggered by lattice heating via multiphoton-generated free electrons may occur at near-infrared wavelengths. At visible wavelengths multiphoton absorption is expected to be the dominant carrier generation process in wide-gap solids. Each of the two breakdown mechanisms thus has its range of operation on the wavelength scale and on the laser pulse length scale. For example, at a wavelength of 1.064 $\mu$m, seven to eight photons are required to cross the forbidden band gap of NaCl and $SiO_2$ in a multiphoton process, excluding multiphoton absorption as an efficient carrier generation process, while it has been shown to be an efficient process at 532 and 266 nm.[6] Mixed cases, where both carrier generation processes are important, are likely under some experimental conditions. A dependence on pulse length arises because impact ionization causes the electron density to increase exponentially with time, while multiphoton absorption causes it to increase linearly with time.[7] A theoretical analysis of these issues requires that the multiphoton-absorption cross section, the impact ionization coefficient, and the free-electron mediated energy transfer rate from the laser field to the lattice must be determined as a function of laser intensity for the wavelength and the solid in question. Multiphoton-absorption cross sections are difficult to calculate, and reliable values have been obtained experimentally only for a few materials at a few wavelengths. The free-electron heating and the electron-multiplication rate, however, can be calculated by solving the Boltzmann transport equation for free electrons in the conduction band in the presence of the laser field. Unfortunately, in order to obtain an analytic solution, Gorshkov, Epifanov, and Manenkov[7] had to make a number of simplifying assumptions which preclude the possibility of making quantitative predictions.

In this paper we present a theoretical study of the interaction of high-power laser radiation at optical and near-infrared wavelengths in wide-gap solids using $SiO_2$ as an example. Our method is based on a Monte Carlo integration of the Boltzmann transport equation for free electrons in the presence of high-intensity optical radiation. Our numerical approach allows for the inclusion of the full energy dependence of the various scattering rates and eliminates many uncertainties arising from approximations necessary to obtain analytically tractable equations in previous theories.[1-5,7] The method allows the simultaneous calculation of the energy transfer from the laser field to the lattice by free-electron heating *and* the calculation of carrier multiplication due to impact ionization in a self-consistent manner. We thus obtain two basic quantities describing the laser-solid interaction which can subsequently be used in a rate-equation approach[7] to calculate the energy transfer from the laser field to the solid or the temperature increase during a high-power laser pulse including the variation of the laser field in space and time.

We apply two different methods for the description of the interaction between the laser field and the free electrons. We use a classical approach, where the laser field is treated as an alternating electric field at the laser frequency, and we use a quantum-mechanical approach by applying second-order perturbation theory. Second-order perturbation theory has previously been applied to semiconductors, for example, to calculate the change of refractive index due to free carriers.[8,9] In most theories of laser breakdown, the laser field has been treated as an alternating electric field. In this approach the quantum nature of the photon field is neglected and the kinetic energy changes continuously in time. Such an approximation is not valid when the average electron energy is small compared to the photon energy, which is the case at low fields and short wavelengths. Sparks *et al.*[10] use the classical approach for the electron-photon interaction at wavelengths $\lambda > 1$ $\mu$m in alkali halides. Similarly, Epifanov[4] and later Gorshkov, Epifanov, and Manenkov[7] estimated that this approach is valid for $E_g/\hbar\omega < 5$, where $\hbar\omega$ is the photon energy and $E_g$ is the band gap of the material. At shorter wavelengths, Gorshkov, Epifanov, and Manenkov[7] have also used a differential-difference kinetic equation to extend their theory to shorter wavelengths. Our study will compare the applicability of the two methods and will show that both methods have limited applicability at visible and near-infrared wavelengths in $SiO_2$.

We have chosen $SiO_2$ as a subject for our numerical calculations for a number of reasons. First, the electron-phonon scattering and impact ionization rates in $SiO_2$ are reasonably well known from direct measurements.[11-13] This is important since any prediction of the theory depends critically on a detailed knowledge of the electron-phonon scattering rates and of the impact ionization rate and their respective energy dependencies.[10] Second, the hot-electron dynamic in $SiO_2$ under high dc electric field, which can be considered as the limit of long laser wave-

length, has been intensely studied experimentally and theoretically.[14–17] It is well established that the simple electron avalanche breakdown model based on polar phonon runaway[18–23] is incorrect in $SiO_2$. The electron energy distribution is known to become unstable and run away from near-thermal energies at 1.5 MV/cm. However, impact ionization does not occur since the electron distribution is restabilized at average electron energies well below the threshold for impact ionization, even for dc electric fields of 6 MV/cm. This happens because the frequency of electron scattering with acoustic phonons increases rapidly with the electron energy. Third, some of the experiments of Jones, Braunlich, Casper, Shen, and Kelly[6] were performed on $SiO_2$, allowing a direct comparison to our calculations.

In Sec. II we discuss the theoretical models used. We only briefly summarize the methods used for the calculation of the electron-phonon scattering rates since our approach in these respects is identical to the methods previously discussed in the context of dc transport in $SiO_2$. The use of second-order perturbation theory for the laser-field–free-electron interaction is discussed in detail. In Sec. III we present typical results of the Monte Carlo simulations in $SiO_2$ for both treatments of the laser-field–free-electron interaction. The two methods are compared and their range of applicability on the wavelength scale is discussed. In Sec. IV we present calculations for realistic laser experiments by incorporating the Monte Carlo transport results into a set of rate equations for the evolution of the free-electron density and of the energy transfer to the lattice. The results are compared to experimental data, and predictions for feasible laser experiments are made. We also discuss limitations and possible extensions of our theory.

## II. THEORY

### A. Monte Carlo simulation and the electron-phonon interaction

The approach used to solve the Boltzmann transport equation in $SiO_2$ is based on the earlier dc Monte Carlo transport formalism of Fischetti.[15,24] The treatment used here is modified mainly with respect to the choice of the phonon scattering rates. The electron states in the conduction band are described in the quasi-free-electron approximation using a single band with one minimum in the extended zone scheme of Sparks *et al.*[10] We thus neglect the detailed atomic structure of $SiO_2$. This approximation yields good results for high-field transport properties even when modeling experiments for amorphous $SiO_2$. Several arguments have been presented to explain this fact. For example, the phonon scattering rates in $SiO_2$ are large, such that the mean free path of electrons is less than 1.5 nm for kinetic energies above 63 meV, the smallest LO-phonon energy. Since amorphous $SiO_2$ has local order on a length scale of 2–3 nm, hot-electron transport is believed to be insensitive to disorder.[25] Density-of-states effects are approximated by using an energy-dependent effective mass. The energy dependence of the mass is derived from measurements of the energy-dependent electron mean free path.

The interactions of the free electrons with the phonons are treated with time-dependent first-order perturbation theory using experimental values for the coupling constants. Polar optical scattering, acoustic phonon scattering, and impact ionization are included. The interaction with the polar optic phonons is treated with the Fröhlich Hamiltonian,[15,26] including the two dominant LO-phonon modes with phonon energies of 63 and 153 meV. Acoustic phonons are included using the deformation-potential theory[15,26] but with the deformation potential going to zero at large wave numbers.[12,27] The electron-phonon coupling constant was determined to be 6 eV from transport experiments. Impact ionization is included via the Keldysh formula:[26]

$$R_{ii}=P\left[\frac{E}{E_{\rm th}}-1\right]^2, \quad E>E_{\rm th}\ . \tag{1}$$

Here, $R_{ii}$ is the impact ionization rate and $E$ is the electron kinetic energy. We have chosen a value of $1.3\times10^{15}$ $s^{-1}$ for the prefactor $P$ and a value of 9 eV for the threshold energy $E_{\rm th}$.[12,27] This choice is in reasonable agreement with the impact ionization rate derived from the dielectric function.[28] The resulting energy dependences of the various scattering rates are summarized in Fig. 1. At energies below 2 eV, the interaction of the electrons with the lattice is primarily via longitudinal-optical (LO) phonons. At higher energies, acoustic scattering rapidly increases and becomes the dominant scattering mechanism. Impact ionization becomes possible at energies above 9 eV. The energy dependences of the phonon scattering rates are similar to those calculated for alkali halides by Sparks *et al.*[10] However, the absolute magnitudes of the various scattering rates, based on direct measurements in $SiO_2$, differ considerably from those in alkali halides. We also use a soft threshold for impact ionization in accordance with experimental data.[13]

The Monte Carlo formalism, in combination with the

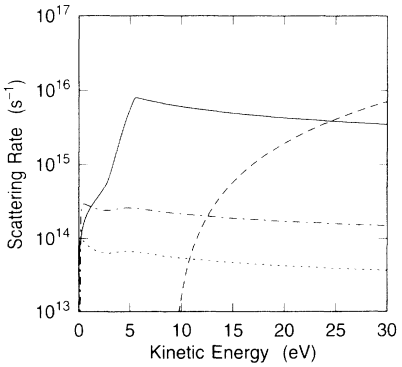


FIG. 1. Electron-phonon scattering rates as a function of kinetic energy. The solid curve is the acoustic-phonon scattering rate, the dot-dashed curve is the LO scattering rate for 153-meV phonons, and the dotted curve is the LO scattering rate for 63-meV phonons. The impact ionization rate is shown by the dashed curve.

scattering rates shown in Fig. 1, has successfully described a wide variety of dc transport experiments in $SiO_2$. These include the average energy as a function of dc electric field measured by electroluminescence,[14] carrier separation,[16] vacuum emission,[17] ballistic transport in thin $SiO_2$ films,[29] high-energy tails in the electron distribution measured by vacuum emission,[17,27] electron escape lengths from soft x-ray photoemission,[11–13] and substrate currents in $n$-channel metal-oxide-semiconductor field-effect transistors (MOSFET's).[27,30] Therefore, the Monte Carlo formalism can be expected to give a reliable description of hot carrier transport in the presence of strong alternating electric fields due to laser radiation.

An alternative model for dc transport in $SiO_2$ has been proposed.[31] This theory employs a model band structure which includes satellite valleys in the conduction band. The dominant scattering mechanism is intervalley scattering via transverse optical phonons rather than acoustic scattering. It is likely that the simple single-band approximation for the $SiO_2$ conduction-band structure is not correct. We believe, however, that the effective mass described above compensates to a large extent for poor knowledge of the actual band structure and that the use of experimentally confirmed energy-dependent scattering rates is responsible for the success of our model.

### B. Laser-field–free-electron interaction

We use two approximations for the interaction of the laser field with the free electrons in the conduction band. The first is the standard classical approach.[1–5,10] The photon field of the laser is treated as a sinusoidal electric field in which the electrons move. The implied assumption is that the photon energy is small compared to the kinetic energy of the electron so that the energy gains and losses from the field may be treated as continuous in time rather than as a series of discrete transitions. We will show later that electrons typically have kinetic energies of about 5 eV for the laser intensities of interest. Therefore, the classical approximation is expected to be valid for long wavelengths only.

To overcome the limitations of the classical approach at short wavelengths, we adopt a quantum-mechanical approach, using second-order time-dependent perturbation theory. The absorption and emission of one photon by a free electron require the simultaneous absorption or emission of a phonon, in order to conserve momentum. We take all phonon modes into consideration. The Hamiltonian for the electron-photon interaction is

$$\mathcal{H}=\frac{e}{m^*}\mathbf{A}\cdot\mathbf{p}\ . \tag{2}$$

Here, $e$ is the electron charge, $m^*$ is the effective electron mass, $\mathbf{p}$ is the electron crystal momentum, and $\mathbf{A}$ is the vector potential of the laser radiation. The total electron energy change, due to both the photon and the phonon, is $\hbar\omega_t$, where $\hbar$ is the reduced Planck constant and $\omega_t$ is the angular frequency. A general expression for the electron-photon–phonon interaction rate can be derived if $\omega_t$ is constant. This can be realized either if the photon energy is large compared to the phonon energy or if the phonon energy can be taken as constant. The free-electron absorption or emission rate $W$ can then be expressed as a function of wave vector $\mathbf{k}$ (Ref. 26):

$$W(\mathbf{k})=\frac{e^2\hbar n_v A_s k^{r+3}}{32\pi\varepsilon_v(\hbar\omega_v)^3 m^*(r+6)} \times\{G_{\max}(\omega_t,E,\beta)-G_{\min}(\omega_t,E,\beta)\}\ . \tag{3}$$

Here, $n_v$ is the photon density, $\varepsilon_v$ is the optical permittivity, and $\omega_v$ is the photon frequency. Equation (3) is valid if the matrix element for the phonon scattering event can be represented as

$$|\langle\mathbf{k}+\mathbf{q}|\mathcal{H}_s|\mathbf{k}\rangle|^2=A_s q^r\ , \tag{4}$$

where $\mathbf{q}$ is the phonon wave vector, $r$ is an integer, and $\mathcal{H}_s$ is the phonon scattering Hamiltonian. The functions $G_m$ are given by

$$G_m=(3\cos^2\beta-1)\left[\frac{q_m}{k}\right]^{r+6}+4(r+6)\left[1-\cos^2\beta-\frac{\hbar\omega_t}{2E}(3\cos^2\beta-1)\right]\left[\frac{1-\delta_{r,-4}}{r+4}\left[\frac{q_m}{k}\right]^{r+4}+\delta_{r,-4}\ln q_m\right] +(r+6)\left[\frac{\hbar\omega_t}{E}\right]^2(3\cos^2\beta-1)\left[\frac{1-\delta_{r,-2}}{r+2}\left[\frac{q_m}{k}\right]^{r+2}+\delta_{r,-2}\ln q_m\right]\ , \tag{5}$$

where $\beta$ is the angle between $\mathbf{A}$ and $\mathbf{k}$. The $\delta$ function is defined by

$$\frac{(1-\delta_{r,x})}{(r-x)}=\begin{cases}0 & \text{if } r=x\\ 1/(r-x) & \text{otherwise}\ .\end{cases} \tag{6}$$

The subscript $m$ on $G$ and $q$ refers to either the maximum or the minimum phonon wave number allowed by energy and momentum considerations. For the case of photon absorption (+) and emission (−), the minimum and maximum phonon wave numbers are given by

$$\frac{q_{\min}}{k}=\left|\left[1\pm\frac{\hbar\omega_t}{E}\right]^{1/2}-1\right|\ , \tag{7}$$

$$\frac{q_{\max}}{k}=\left[1\pm\frac{\hbar\omega_t}{E}\right]^{1/2}+1 \ . \tag{8}$$

In both cases, $\hbar\omega_t$ is a positive quantity and for emission it must be less than the kinetic energy.

Given the matrix elements corresponding to the various electron-phonon interactions, one can determine the corresponding optical absorption and emission rates. Using the Fröhlich Hamiltonian for the interaction of electrons with polar phonons gives for $A_s$ and $r$,

$$A_s q^r=\frac{e^2\hbar\omega_{\rm LO}}{2V\varepsilon_p q^2}n^*(\omega_{\rm LO}) \ . \tag{9}$$

Here, $\hbar\omega_{\rm LO}$ is the LO-phonon energy, $n^*$ is the phonon occupation number for phonon absorption and the occupation number $+1$ for phonon emission, $V$ is the crystal volume, and $1/\varepsilon_p=1/\varepsilon_\infty-1/\varepsilon_0$, where $\varepsilon_\infty$ and $\varepsilon_0$ are the high- and low-frequency permittivity, respectively. We neglect the dispersion in the LO-phonon energy. Inserting Eq. (9) into Eq. (3) thus yields for photon absorption $(+)$ or emission $(-)$

$$W_\pm=\frac{e^4 n_v\hbar\omega_{\rm LO}(2E)^{1/2}}{256\pi\varepsilon_v m^{*1/2}(\hbar\omega_v)^3\varepsilon_p}n^*(\omega_{\rm LO})$$
$$\times\left\{\frac{16}{3}\left[\left[\frac{q_{\max}}{k}\right]^2-\left[\frac{q_{\min}}{k}\right]^2\right]+(3\cos^2\beta-1)\left\{\left[\frac{q_{\max}}{k}\right]^4-\left[\frac{q_{\min}}{k}\right]^4\mp 8\left[\frac{\hbar\omega_t}{2E}\pm\frac{1}{3}\right]\left[\left[\frac{q_{\max}}{k}\right]^2-\left[\frac{q_{\min}}{k}\right]^2\right]\right.\right.$$
$$\left.\left.+4\left[\frac{\hbar\omega_t}{E}\right]^2\ln\left[\frac{q_{\max}}{q_{\min}}\right]\right\}\right\} . \tag{10}$$

Acoustic phonons are treated by the deformation-potential theory. We consider a linear phonon-energy dispersion for normal processes and use the zone-edge value for phonons with larger wave numbers.[10,15] The matrix element for normal acoustic phonons using equipartition is

$$A_s q^r=\frac{C^2 k_B T}{2\rho c_s^2 V} \ . \tag{11}$$

$C$ is the deformation-potential constant, $k_B$ is Boltzmann's constant, $T$ is the absolute temperature, $\rho$ is the crystal density, and $c_s$ is the speed of sound in the material. Using this matrix element in Eq. (3) yields for photon absorption $(+)$ and emission $(-)$,

$$W_\pm=\frac{e^2 n_v C^2 k_B T(2m^*)^{1/2}E^{3/2}}{192\pi\varepsilon_v(\hbar\omega_v)^3\hbar^2\rho c_s^2}\left\{4\left[\left[\frac{q_{\max}}{k}\right]^4-\left[\frac{q_{\min}}{k}\right]^4\right]+(3\cos^2\beta-1)\left\{\left[\frac{q_{\max}}{k}\right]^6-\left[\frac{q_{\min}}{k}\right]^6\right.\right.$$
$$\mp 6\left[\frac{\hbar\omega_t}{2E}\pm\frac{1}{3}\right]\left[\left[\frac{q_{\max}}{k}\right]^4-\left[\frac{q_{\min}}{k}\right]^4\right]$$
$$\left.\left.+3\left[\frac{\hbar\omega_t}{E}\right]^2\left[\left[\frac{q_{\max}}{k}\right]^2-\left[\frac{q_{\min}}{k}\right]^2\right]\right\}\right\} . \tag{12}$$

In Eq. (12) it was assumed that the phonon energy is small compared to the photon energy. This assumption is clearly fulfilled in circumstances for which second-order perturbation theory is valid. For acoustic umklapp processes, we instead take the zone-edge phonon $\omega_{\rm BZ}$:

$$A_s q^r=\frac{\hbar C^2}{2\rho c_s^2 V}n^*(\omega_{\rm BZ}) \ . \tag{13}$$

The photon absorption $(+)$ and emission $(-)$ rate is given by

$$W_\pm=\frac{e^2 n_v C^2 m^* E^2}{112\pi\varepsilon_v(\hbar\omega_v)^3\hbar^2\rho c_s^2}n^*(\omega_{\rm BZ})$$
$$\times\left\{\frac{56}{15}\left[\left[\frac{q_{\max}}{k}\right]^5-\left[\frac{q_{\min}}{k}\right]^5\right]+(3\cos^2\beta-1)\left\{\left[\frac{q_{\max}}{k}\right]^7-\left[\frac{q_{\min}}{k}\right]^7\mp\frac{28}{5}\left[\frac{\hbar\omega_t}{2E}\pm\frac{1}{3}\right]\left[\left[\frac{q_{\max}}{k}\right]^5-\left[\frac{q_{\min}}{k}\right]^5\right]\right.\right.$$
$$\left.\left.+\frac{7}{3}\left[\frac{\hbar\omega_t}{E}\right]^2\left[\left[\frac{q_{\max}}{k}\right]^3-\left[\frac{q_{\min}}{k}\right]^3\right]\right\}\right\} . \tag{14}$$

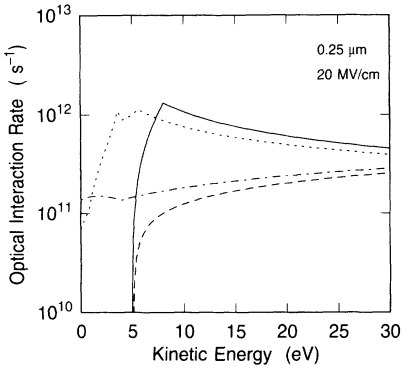


FIG. 2. The electron-photon interaction rate for a wavelength of 250 nm, an intensity of 1 TW cm$^{-2}$, and the electron crystal momentum parallel to the vector potential of the laser radiation calculated in second-order perturbation theory. The dotted curve is the photon absorption rate assisted by acoustic phonons, the solid curve is the photon emission rate assisted by acoustic phonons, the dot-dashed curve is the photon absorption rate assisted by LO phonons, and the dashed curve is the photon emission rate assisted by LO phonons.

In the Monte Carlo simulation, all these scattering rates must be calculated for each laser intensity and laser wavelength at all possible values for the angles $\beta$ between the laser field and the electron momentum. As a typical example, we show in Fig. 2 the optical interaction rates for a laser wavelength of 250 nm and an intensity of 1 TW/cm$^2$. The electron crystal momentum is parallel to the vector potential. For kinetic energies larger than about 1 eV, the dominant terms are due to acoustic-phonon-assisted interactions. This remains true for all combinations of laser intensity, wavelength, and angle $\beta$. Note that the optical interaction rates and the corresponding electron-phonon scattering rates have a somewhat similar dependence on kinetic energy.

The Boltzmann transport formalism is valid only if the distance between collisions is sufficiently large such that the scattering can be treated as independent events. From Eq. (3) one can see that the optical interaction rates increase with the third power of the wavelength. Therefore, above some critical wavelength, the total photon emission and absorption rates become too large and the quantum-mechanical interference between collision events can no longer be neglected. A quantitative comparison of the two approximations will be made in Sec. III C.

## III. MONTE CARLO TRANSPORT RESULTS

In this section we present typical steady-state transport results of free electrons in the conduction band of $SiO_2$. We calculate the electron energy distribution, average electron energies, the energy transfer rate from the laser field to the lattice (free-electron heating), and the impact-multiplication rate self-consistently. These quantities are calculated as a function of laser intensity and laser wavelength. We will show that the use of a steady-state calculation is justified for laser pulses of durations longer than about 100 ps. For shorter pulses the electron energy distribution will not follow the time variation of the electric field or the photon field in a quasi-steady-state fashion. For longer pulses, the variation of the laser pulse in time and space can subsequently be included in a rate-equation approach which uses the values of our steady-state calculation as input parameters. Examples are presented in Sec. IV.

### A. Classical results

The instantaneous kinetic energy of a sample electron in an alternating electric field is shown in Fig. 3. This calculation was done for a laser wavelength of 10 $\mu$m and the zero-to-peak electric-field amplitude of 20 MV/cm, which corresponds to an intensity of 770 GW/cm$^2$ using

$$I=\tfrac{1}{2}F^2ny \ , \tag{15}$$

where $F$ is the zero-to-peak electric-field amplitude, $n$ is the refractive index, and $y$ is the admittance of free space (0.002 66 Fs$^{-1}$). Figure 3 demonstrates that the energy is well randomized on the time scale of 1 ps. The electron energy distribution will therefore adjust to a change of the laser field on the ps time scale in a quasi-steady-state fashion, and quantities calculated under steady-state conditions allow an accurate description of effects by laser pulses on the order of 100 ps or longer. The laser field also varies in space, and strong heating and damage occurs in a region where the laser is most strongly focused. Typical dimensions of laser beams are on the order of 1 $\mu$m. Separate calculations show that this distance is large compared to the electron diffusion length, and spatial variations of the field can be reliably determined from steady-state, spatially invariant calculations.

The electron density functions are calculated from the time average of one sample electron over a time period of typically 1 ns using a homogeneous field in space. Results for $\lambda=10$ $\mu$m and for peak electric-field amplitudes of 2, 10, 20, and 30 MV/cm are shown in Fig. 4. In all cases, the majority of the electrons are below 5 eV in en-

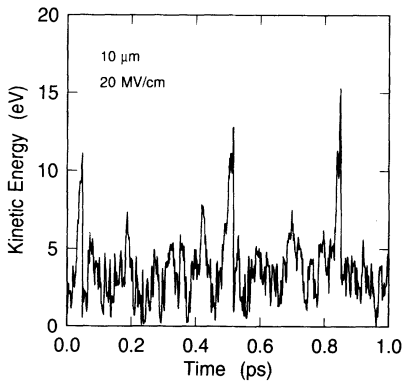


FIG. 3. The calculated instantaneous kinetic energy of a sample electron as a function of time. The classical approach is used for the laser-field–free-electron interaction. The laser wavelength is 10 $\mu$m and the zero-to-peak electric-field amplitude is 20 MV cm$^{-1}$.

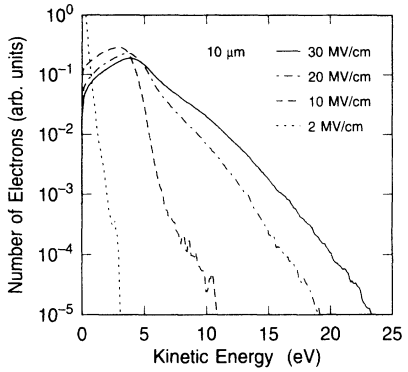


FIG. 4. The calculated density of electrons as a function of kinetic energy for a laser wavelength of 10 $\mu$m. The classical approach is used for the laser-field–free-electron interaction. Curves are shown for zero-to-peak fields ranging from 2–30 MV cm$^{-1}$.

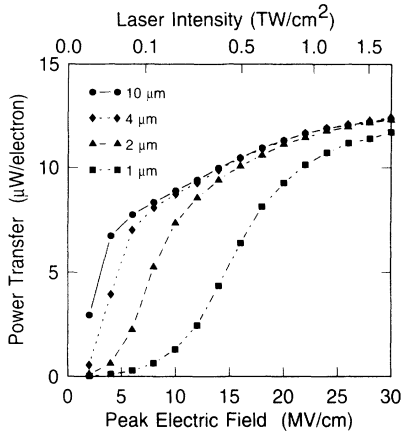


FIG. 6. The calculated power transfer from the electron population to the lattice as a function of zero-to-peak electric field (or equivalent laser intensity). The classical approach is used for the laser-field–free-electron interaction. Curves are shown for wavelengths of 1–10 $\mu$m.

ergy. However, a high-energy tail starts to form for fields of about 10 MV/cm or larger, and impact ionization becomes possible. This can also be seen in Fig. 3, where three impact ionization events occurred at times of approximately 0.05, 0.5, and 0.85 ps. Due to the soft threshold for impact ionization, the electrons can have kinetic energies above the ionization threshold of 9 eV. The electrons gain such large amounts of energy by chance in-phase scattering with the electric field. Only such rare events contribute to the high-energy tail of the electron distribution above the impact ionization threshold and can excite electron-hole pairs.

In Fig. 5 the average electron energies are shown as a function of electric field at wavelengths of 1, 2, 4, and 10 $\mu$m. These data show that there exists a threshold field for strong electron heating which rapidly shifts to higher field values at shorter wavelengths. The electrons remain at near-thermal energies, simply moving back and forth at the frequency of the electric field, until the field amplitude becomes large enough to accelerate the electron to energies at which the acoustic scattering rate is appreciable (see Fig. 1). At these higher energies, large-angle scattering in phase with the ac field becomes possible since acoustic scattering, unlike polar-phonon scattering, randomizes the momentum of an electron. We find that the distribution functions in Fig. 4 and the average energies for the 10-$\mu$m case are quantitatively similar to dc results using field values equal to the corresponding root-mean-square (rms) electric fields. This indicates that the dc limit is essentially reached for large electric fields at 10 $\mu$m. This is not surprising, since the period of the electric field, $3.3\times10^{-14}$ s, is large compared to the total phonon scattering time (see Fig. 1).

An important quantity is the rate at which electrons transfer heat to the lattice. In steady state this is also the rate at which electrons absorb energy from the laser radiation. This power transfer per electron is shown in Fig. 6

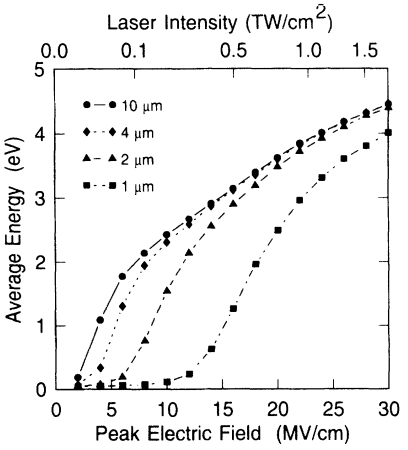


FIG. 5. The calculated average kinetic energy as a function of zero-to-peak electric field (or equivalent laser intensity). The classical approach is used for the laser-field–free-electron interaction. Curves are shown for wavelengths of 1–10 $\mu$m.

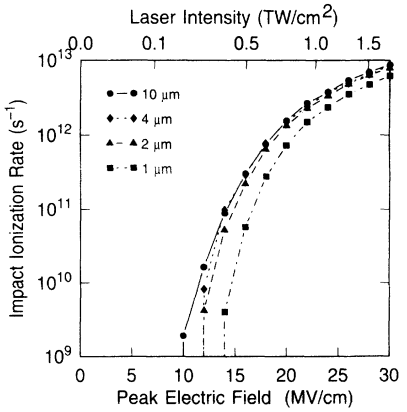


FIG. 7. The calculated impact ionization rate as a function of zero-to-peak electric field (or equivalent laser intensity). The classical approach is used for the laser-field–free-electron interaction. Curves are shown for wavelengths of 1–10 $\mu$m.

as a function of field and wavelength. There are two contributions to this transfer. The contribution due to polar-optic phonons is almost constant with electron energy, though actually slowly decreasing. In contrast, the contribution due to acoustic phonons increases rapidly with energy above 1 eV and peaks at about 6 eV, in a manner consistent with the scattering rates in Fig. 1. The combined result is a transfer of power to the lattice which increases with electron kinetic energy and shows a functional dependence on the peak field similar to that found for the average electron energy. The impact ionization rate as a function of electric field is shown in Fig. 7 for laser wavelengths of 1, 2, 4, and 10 $\mu$m. Again, the 10-$\mu$m data approach the results of dc calculations at the corresponding rms fields.

### B. Quantum-mechanical results

Section III A concentrated on the long-wavelength results where the classical theory is most valid. The quantum-mechanical theory is most valid at short wavelengths where the optical absorption and emission rates are low. In Fig. 8 the instantaneous kinetic energy is shown for a time interval of 1 ps at a zero-to-peak electric-field intensity of 20 MV/cm. In this example the electron absorbs photons ($\lambda=250$ nm) at approximately 0.35 and 0.7 ps. In between absorption events, the kinetic energy decreases due to phonon emission. Here optical interactions are infrequent compared to phonon scattering events, but the interactions result in a dramatic change in the kinetic energy. This is considerably different from the classical results at 10 $\mu$m shown in Fig. 3. The large and relatively infrequent jumps in energy seen in Fig. 8 are reflected directly in the energy densities shown in Fig. 9. Well-defined drops in the density of electrons can be seen near the conduction-band minimum, and again at an energy equal to one photon energy. The rapid decrease near zero kinetic energy occurs because the electrons must absorb a photon to get significantly above thermal energies. To get above 5 eV

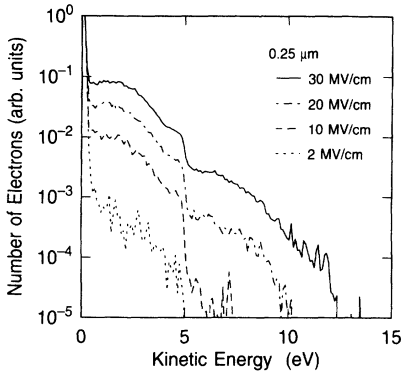


FIG. 9. The calculated density of electrons as a function of kinetic energy for a laser wavelength of 250 nm. The quantum approach is used for the laser-field–free-electron interaction. Curves are shown for zero-to-peak fields ranging from 2–30 MV cm$^{-1}$.

of energy, the electron must absorb a second photon before it loses its energy due to either phonon or photon emission. These sudden drops in the electron density are less dramatic at larger electric-field amplitudes since the optical interaction rates increase quadratically with the electric-field amplitude. Again, a high-energy tail begins to form at peak electric fields larger than about 10 MV/cm.

The power transfer from the electron to the lattice is plotted in Fig. 10 as a function of field amplitude at wavelengths of 250 nm, 500 nm, and 1.0 $\mu$m. The strong dependence of the power transfer on wavelength reflects the cubic dependence in the optical interaction rates in Eq. (3). This strong wavelength dependence is even more noticeable in the impact ionization rates shown in Fig. 11. The dramatic reduction of the impact ionization rate and the corresponding shift of the ionization threshold towards higher fields at short wavelength gradually elimi-

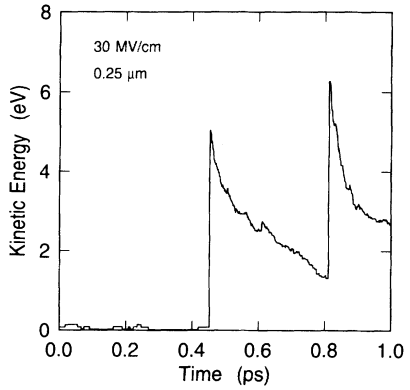


FIG. 8. The calculated instantaneous kinetic energy of a typical electron as a function of time. The quantum approach is used for the laser-field–free-electron interaction. The laser wavelength is 250 nm and the zero-to-peak electric-field amplitude is 30 MV cm$^{-1}$.

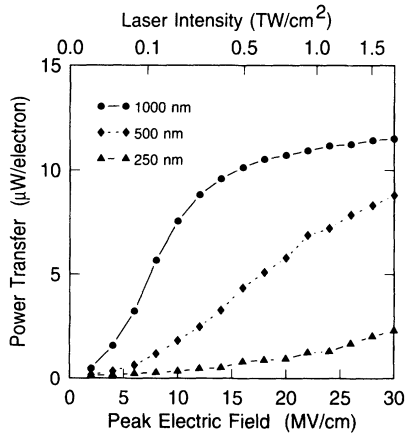


FIG. 10. The calculated power transfer from the electron population to the lattice as a function of zero-to-peak electric field (or equivalent laser intensity). The quantum approach is used for the laser-field–free-electron interaction. Curves are shown for wavelengths of 250 nm–1 $\mu$m.

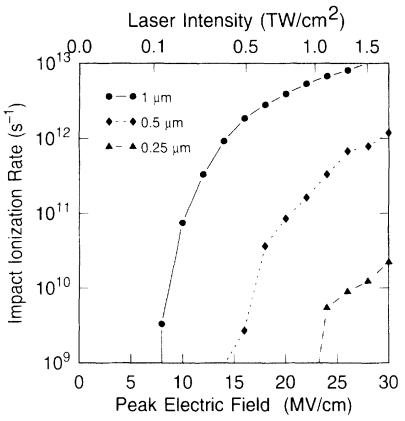


FIG. 11. The calculated impact ionization rate as a function of zero-to-peak electric field (or equivalent laser intensity). The quantum approach is used for the laser-field–free-electron interaction. Curves are shown for wavelengths of 250 nm–1 $\mu$m.

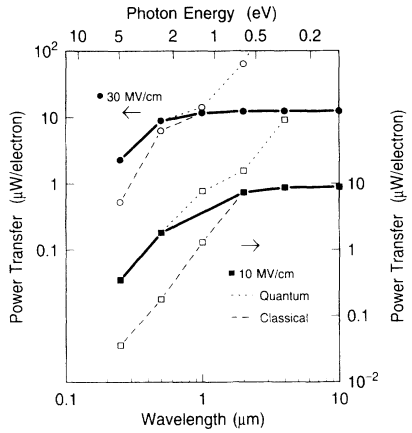


FIG. 13. The calculated power transfer from the electrons to the lattice as a function of laser wavelength. Results due to both the classical and the quantum-mechanical treatment of the electron-photon interaction are shown for zero-to-peak electric fields of 10 and 30 MV cm$^{-1}$. The transition from the quantum regime at short wavelengths to the classical regime at long wavelengths is interpolated qualitatively, as shown by the heavy line.

nate impact ionization as a free-electron generation process.

### C. Comparison of classical and quantum results

Based on the qualitative discussion in Sec. II, it is expected that the classical model will fail at short wavelengths and the quantum-mechanical model will fail at long wavelengths. These trends are quantitatively confirmed by our simulations as summarized in Figs. 12–14. In Fig. 12 the average kinetic energies calculated by the two methods are compared at various wavelengths. The dashed curves show data using the classical approach at zero-to-peak electric-field amplitudes of 10 MV/cm (squares) and 30 MV/cm (circles), respectively. The dotted curves show data using the quantum-mechanical approach at the same field values. The results show a qualitatively similar wavelength dependence at both field values. We discuss the 10-MV/cm case which shows the differences between the two methods more clearly. In the classical calculation, the average energy saturates at long wavelengths at the value in the dc limit. Below 2 $\mu$m, the classical results rapidly deviate from the long-wavelength limit and the average energy decreases to near the thermal equilibrium value. In simple terms, this rapid transition occurs because the laser

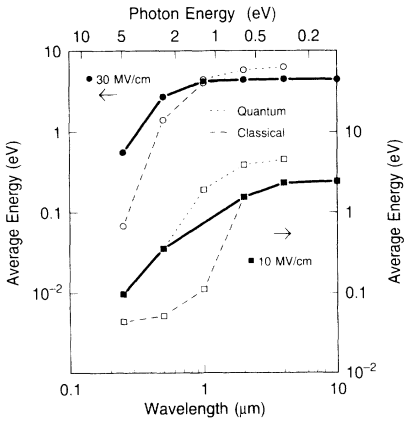


FIG. 12. The calculated average kinetic energy as a function of laser wavelength. Results due to both the classical and the quantum-mechanical treatment of the electron-photon interaction are shown for zero-to-peak electric fields of 10 and 30 MV cm$^{-1}$. The transition from the quantum regime at short wavelengths to the classical regime at long wavelengths is interpolated qualitatively, as shown by the heavy line.

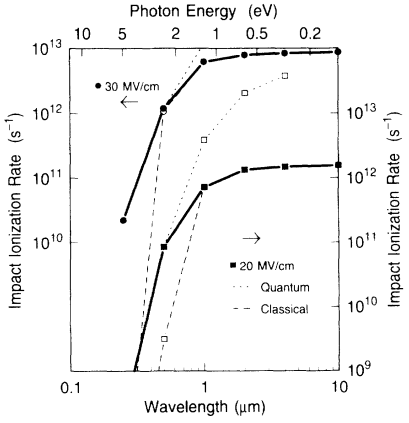


FIG. 14. The calculated impact ionization rate as a function of laser wavelength. Results due to both the classical and the quantum-mechanical treatment of the electron-photon interaction are shown for zero-to-peak electric fields of 20 and 30 MV cm$^{-1}$. The transition from the quantum regime at short wavelengths to the classical regime at long wavelengths is interpolated qualitatively, as shown by the heavy line.

frequency becomes much larger than the acoustic-phonon scattering rate, making large-angle scattering in phase with the electric field impossible. The electrons simply oscillate at high frequency near thermal equilibrium without gaining energy. The strong energy dependence of the phonon scattering rate complicates this simple picture. At higher field amplitudes (see the 30-MV/cm case in Fig. 12), the energy oscillations at the same frequency are large enough to accelerate the electrons to sufficiently high energy (and sufficiently high acoustic scattering rates) that in-phase scattering becomes more likely. At high fields, the transition to the dc limit gets shifted to shorter wavelengths. This behavior cannot be obtained properly from an average electron model since the energy dependence of the scattering rates would not then be fully included. At all wavelengths, the quantum-mechanical method gives a higher average energy than the classical method. Clearly, the large average energies obtained at long wavelengths are not physically reasonable since these values exceed the result in the dc limit. As discussed above, this divergence is due to the fact that the scattering rates become so large that an adequate description of the electron transport with the semiclassical Boltzmann equation is no longer possible. At short wavelengths, the scattering rates are low enough for the quantum-mechanical treatment to be valid, and the higher values for the average electron energy as compared to the classical results are accurate. At 10 MV/cm, both approximations fail at wavelengths of the order of 1 $\mu$m since the quantum-mechanical method becomes inaccurate with increasing wavelength before the classical method yields correct values and there is no overlapping wavelength range in which both methods yield the same results. Therefore, only estimates for the average electron energy can be derived in the wavelength range around 1 $\mu$m. The two methods yield an upper and lower bound to the actual average energy. In Fig. 12 we assume the quantum-mechanical results to be valid up to wavelength $\lambda=500$ nm and the classical results down to $\lambda=2.0$ $\mu$m, and we interpolate the results in the intermediate range as shown. It is interesting that the two methods tend to converge in the intermediate-wavelength range at high fields (see the 30-MV/cm calculations in Fig. 12). This happens because the validity range of the classical method is extended to lower wavelengths. The reason is that at large fields, electron heating is stronger and the average energies remain large in comparison to the photon energy down to lower wavelengths. Apparently, the criterion of $E_g > 5\hbar\omega$ for the range of validity suggested by Epifanov and co-workers[4,7] for the classical treatment of the electron-photon interaction is not strict enough. Requiring $E_{\text{ave}} > 5\hbar\omega$ would be more appropriate. This latter condition is observed for 1-$\mu$m radiation in $SiO_2$ only for the largest intensities considered in this study.

The above discussion on the wavelength dependence of the average energies essentially applies to the power transfer shown in Fig. 13 as well. The failure of the quantum-mechanical method at long wavelengths can be seen in a more dramatic way here. The values for the power transfer become much larger than the values obtained by the classical method. The quantum results even appear to diverge in the dc limit. This effect is due to an overestimation of the energy transfer by the second-order photon-phonon-electron interactions. If the power transfer is determined only from the first-order phonon scattering processes, then the power transfer is virtually identical to the values obtained by the classical method at long wavelengths. The calculated values for the impact ionization rates are summarized in Fig. 14. Results are shown for field values of 20 and 30 MV/cm. Again, the discussion given for the average energies applies to the results for the impact ionization rate except that the field dependence is more pronounced as it depends on the high-energy tail of the energy distribution rather than the peak of the distribution. Therefore, we find an extremely strong decrease in the impact ionization rate at short wavelengths which is more pronounced than the decrease found in the power transfer. Lattice heating by free electrons remains fairly efficient at wavelengths where impact ionization is dramatically reduced. This last finding is important for the understanding of experimental results as illustrated in Sec. IV.

## IV. COMPARISON WITH EXPERIMENTS

In this section we calculate the effects of high-intensity laser pulses in $SiO_2$ by solving the rate equation for the evolution of the free-electron density, $n(t)$, during a realistic laser pulse, including the variation of the zero-to-peak field with space and time. From the evolution of the free-electron density, we calculate the total-energy transfer $\Delta E$ and the corresponding temperature increase in the solid. As shown in Sec. III, the impact ionization rates and the energy transfer rates obtained from steady-state calculations can be used in rate equations for pulse durations of the order of 100 ps or greater and a focal waist radius of the order of 1 $\mu$m or larger. We consider pulses of about 100 ps here, and neglect heat diffusion during the pulse.

The evolution of the free-electron density $n(t)$, and the energy transfer from the laser field to the lattice by free electrons $\Delta E(t)$, during a laser pulse under the above conditions can be obtained from a set of rate equations of the form[4,7]

$$\frac{dn}{dt} = W_m(F) + \gamma(F)n - R(F,n) \tag{16}$$

and

$$\frac{d\Delta E}{dt} = P(F)n \ , \tag{17}$$

where $\gamma$ is the ionization rate, $W_m$ is the $m$-photon generation rate, $R$ is the carrier recombination rate, and $P$ is the power transfer per electron. Note that $\gamma$ is related to the ionization coefficient $\beta$, as $\gamma=\ln(2)\beta$. $W_m$ can be expressed in terms of the generalized multiphoton-absorption cross section $\sigma^{(m)}$ as[6]

$$W_m = \sigma^{(m)} n_i \Phi^m \ . \tag{18}$$

Here, $n_i$ is the active ion density with a value of

$2.1\times10^{21}$ cm$^{-3}$ and $\Phi$ is the photon flux. The net temperature increase $\Delta T$ is simply calculated from the total-energy transfer using the equation $\Delta E = c\rho\Delta T$, where $c$ is the specific heat and $\rho$ is the density.

The differential equations are solved numerically using a fourth-order Runge-Kutta method. The spatial variation of the laser intensity is modeled as a focused beam with a Gaussian profile described by a waist radius $\omega_0$ and the confocal parameter $z_0 = 2\pi\omega^2 n_r/\lambda$, where $n_r$ is the refractive index and $\lambda$ the laser wavelength. A Gaussian intensity profile is also used in the time domain with a $1/e$ width of $\tau_0$. For the integration over space, the equations are solved for small volume elements with constant zero-to-peak field. The power transfer per electron and the impact ionization rate at the instantaneous peak field are interpolated from data similar to that shown in Figs. 10 and 11.

In a first example, we examine the importance of impact ionization as a free-carrier generation process at a wavelength of 500 nm. We neglect carrier recombination. In Fig. 15 the calculated temperature increase in the focal point is shown as a function of photon flux (intensity) for typical values of the four-photon absorption cross section $\sigma^{(4)}$.[6] The dotted curves show the results without impact ionization, $\gamma = 0$; the solid lines show the result with both carrier generation processes included. This simple calculation allows several interesting conclusions regarding the high-power laser interaction with $SiO_2$. First, the temperature increase and the total-energy transfer to the lattice (calculated but not shown here), and consequently the photoacoustic signal (assuming that it is proportional to the total-energy transfer), all follow approximately a fifth-order power law. This is surprising considering that the carrier generation mechanism is fourth order. This fifth-order dependence arises simply from the combined effect of the fourth-order generation rate and an approximately first-order dependence of the energy transfer rate on photon flux, as shown in Fig. 10. In alkali halides, a fourth-order flux dependence for the photoacoustic signal was observed for materials with a four-photon band gap.[6] We can only speculate on the origin of this difference. Carrier recombination may play an important role. Also, the power transfer may have a weaker photon flux (intensity) dependence in the alkali halides. The important point is that the power dependence of the temperature increase (or the photoacoustic signal) does not necessarily reflect the order of the multiphoton excitation process. For reasonable values for $\sigma^{(4)}$ of the order of $1\times10^{-114}$ cm$^8$ s$^3$ [in NaCl, KBr, and KI, values of $1.5\times10^{-114}$, $(2\pm1)\times10^{-114}$, and $(2\pm0.8)\times10^{-114}$ cm$^8$ s$^3$ have been measured, respectively[6]], the calculation in Fig. 15 predicts that the solid will reach its melting point at intensities that are far too low for any significant carrier multiplication by impact ionization to occur. This conclusion is perfectly consistent with several experiments of Jones *et al.*[6] which show that impact ionization plays at most a minor role in four-photon band-gap materials at 500 nm wavelength.[6] Only for much lower values of $\sigma^{(4)}$ do we predict significant carrier generation by impact ionization, leading to a clear deviation from the fifth-order laser energy dependence in the data shown in Fig. 15. Also shown in Fig. 15 is the result of a calculation (dashed line labeled "zero") with impact ionization as the only carrier generation mechanism. One starting electron per cm$^3$ is used in all cases. As can be seen, the temperature increases extremely fast in the absence of multiphoton absorption, leaving no measurable precursors at sub-breakdown pulse energies. All these calculations strongly suggest that multiphoton absorption and free-carrier heating play a dominant role for breakdown in $SiO_2$ at wavelengths of 500 nm or shorter and that energy deposition and lattice heating should occur well below the impact ionization threshold.

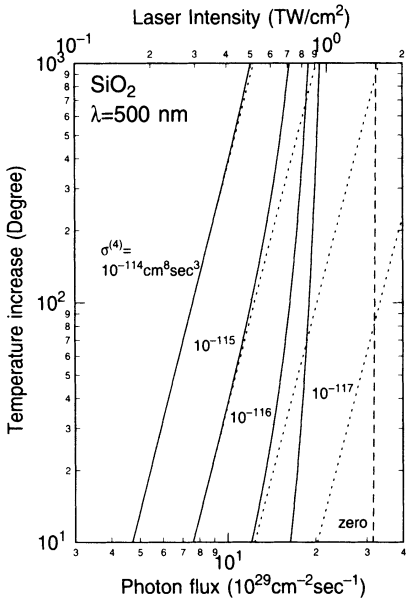


FIG. 15. Calculated temperature increase in $SiO_2$ as a function of peak photon flux (or equivalent laser peak intensity) due to a 100-ps laser pulse at a wavelength of 500 nm using different values of the four-photon generation cross section, $\sigma^{(4)}$. The solid curves were obtained with both multiphoton absorption and impact ionization included as carrier generation mechanisms. The dotted curves show results without impact ionization. The dashed curve (labeled zero) is the result for the avalanche breakdown model, $\sigma^{(4)} = 0$.

In a second example, the temperature increase in $SiO_2$ due to a 100-ps laser pulse at $\lambda = 1$ $\mu$m is estimated. Again, carrier recombination is neglected. We further neglect multiphoton absorption by the 1-$\mu$m pulse since $SiO_2$ has a seven-to-eight-photon band gap at this wavelength. We are thus left with the avalanche breakdown model. We use the quantum results for the power transfer. The calculated temperature increases as a function of peak intensity for different values of the starting electron density, $n_0$, are shown in Fig. 16. A density of $1\times10^{15}$ cm$^{-3}$ or smaller is typically assumed in avalanche breakdown models. Clearly, the temperature increase is explosive, and little lattice heating at pre-breakdown laser intensities is predicted under this condition. For higher starting electron densities, the situation dramatically changes. The power transfer per electron is large enough to cause a significant temperature increase

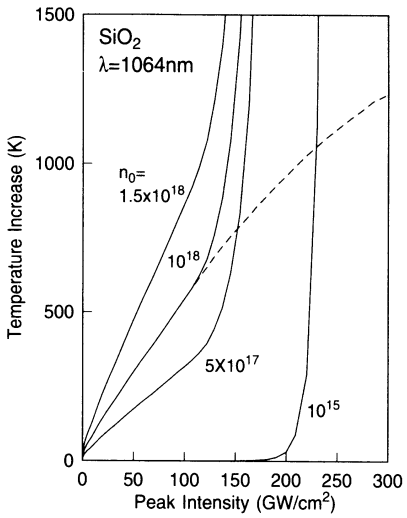


FIG. 16. Calculated temperature increase in $SiO_2$ as a function of laser peak intensity due to a 100-ps pulse at a wavelength of 1 $\mu$m using different values for the starting electron density, $n_0$. The dashed curve was obtained by neglecting impact ionization with $n_0 = 10^{18}$ cm$^{-3}$.

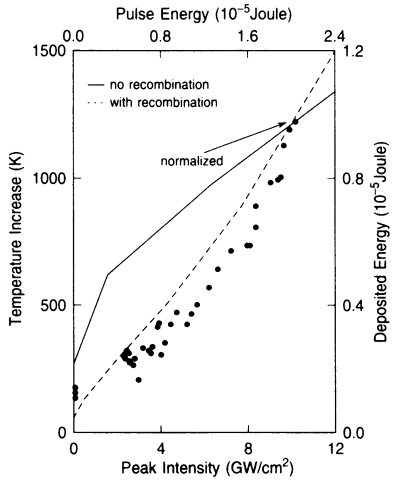


FIG. 17. The temperature increase and the corresponding energy transfer from the laser field to the lattice as a function of laser peak intensity or equivalent pulse energy for the pulse conditions in the two-wavelength experiment described by Jones *et al.* in Ref. 6. The experimental data (dots) show the photoacoustic signal generated by a 1.064-$\mu$m heat pulse following a 266-nm pump pulse used for free-carrier generation. The calculations shown by the solid (dashed) line were obtained by using a three-photon absorption cross section of $2\times10^{-81}$ cm$^6$s$^2$ ($5\times10^{-81}$ cm$^6$s$^2$) and neglecting (including) electron-hole pair recombination. For details see the text.

at fairly low peak intensities, as shown by the solid lines. At about 130 GW/cm$^2$, impact ionization sets in and the temperature increase is enhanced due to carrier multiplication. The dotted line shows the hypothetical evolution of the lattice temperature in the absence of impact ionization for a starting carrier density of $1\times10^{18}$ cm$^{-3}$. Without carrier recombination, the temperature increase is proportional to the starting electron density. From Fig. 16 it can thus be seen that it is necessary to generate a free-electron density of $\approx 2\times10^{18}$ cm$^{-3}$ by a pump pulse in a two-pulse experiment in order to melt the solid by a subsequent laser pulse at 1 $\mu$m without any assistance of carrier multiplication by impact ionization.

In a last example, we compare our calculations directly with the two-pulse experiments of Jones *et al.*[6] Their result is shown in Fig. 17. The pump pulse alone produces a photoacoustic signal which is about $\frac{1}{8}$ of the signal at breakdown, and the signal increases approximately with the third power of the heat pulse energy. These data were measured under the following experimental conditions.[32] The energy and the waist radius of the 266-nm pump pulse were $5.5\times10^{-6}$ J and 4 $\mu$m. For the 1.064-$\mu$m heat pulse, these parameters were $23\times10^{-6}$ J and 26 $\mu$m. The pulse length was approximately 100 ps. These parameters imply a maximum zero-to-peak field of 8 MV/cm for the pump pulse and of 3 MV/cm for the heat pulse. Comparison of these field values with the ionization rates in Fig. 11 shows that impact ionization does not occur and that the lattice heating is not related to impact ionization. We calibrate the photoacoustic signal as follows: We assume the signal to be proportional to the total deposited energy. We also assume that the crystal breaks down thermomechanically due to excess Joule heating or melting. A net temperature increase in the focal volume of 1200 K is assumed to be necessary for this to happen. The uncertainty in the temperature increase required for breakdown to occur leaves the calibration of the acoustic signal uncertain within a factor of about 2. We then solve the rate equations using the Monte Carlo results obtained with the quantum approach, neglecting recombination. The above temperature condition at breakdown can be satisfied with a value of $2\times10^{-81}$ cm$^6$s$^2$ for the three-photon generation cross section, as shown by the solid curves in Fig. 17. This value falls well within the range of measured three-photon cross sections in other materials.[6] Lattice heating is much less efficient at 266 nm than at 1.064 $\mu$m, as can be seen from Fig. 11, but still efficient enough to yield the measured offset in the photoacoustic signal in the absence of the heat pulse. If we use the power transfer per electron as calculated by the classical approach for the laser field, lattice heating can be neglected for the experimental conditions used above and the two-pulse experiments cannot be explained. This is not surprising. At low intensities, the average electron energies are comparable to the photon energies even at 1 $\mu$m, and the classical approach is inaccurate.

The dependence of the deposited energy on the laser intensity, shown in Fig. 17, does not agree with the functional form of the photoacoustic signal. This incompatibility is most likely due to the neglect of electron-hole recombination in the calculation, as demonstrated with a delay experiment.[6] Lattice heating was found essentially to vanish at a delay of 200–300 ps between the two pulses due to the rapid decay of the free-electron density via electron-hole recombination. Little is known of the recombination rates in $SiO_2$ under strong electric fields at

optical frequencies. Williams, Klein, and Marquardt[33] showed that electron-hole recombination in alkali halides occurs on a picosecond time scale and that the carrier lifetime is a strong function of the carrier concentration. A similar behavior can be expected in $SiO_2$. To illustrate the effect of carrier recombination in such an experiment, we use the electron capture cross section of trapped holes (Coulombic trapping centers) under strong dc fields in $SiO_2$, as measured by Buchanan, Fischetti, and DiMaria[34] as an estimate for electron-hole recombination and its field dependence. These authors showed that electron heating at high dc fields strongly reduces the capture cross section. Since the electron heating at 1 $\mu$m is comparable to electron heating in a dc field with a field value equal to the rms field of the ac field, as shown in Sec. III, the absolute values for the capture cross section can be expected to depend on field in a similar fashion in both cases. In $SiO_2$, the mobility of holes is much smaller than the mobility of electrons. We assume the holes to be stationary and use first-order kinetics for the electron-hole recombination. The recombination rate is given by

$$R(F)=\sigma_c(F)v_e n_e n_h \ . \tag{19}$$

Here, $\sigma_c$ is the Coulombic capture cross section with a field dependence of $F^{-1.5}$ for $F<1.2$ MV/cm and $F^{-3}$ for $F\geq 1.2$ MV/cm.[34] The quantity $v_e$ is an effective velocity (the drift velocity in the dc case at low fields). The hole density $n_h$ is equal to the electron density $n_e$ in our case. The velocity term in Eq. (19) is not known. The high-field drift velocity which is of the order of $10^7$ V/cm can be taken as an upper limit. Using this recombination model, we obtain the dashed lines in Fig. 17 using $5\times 10^{-81}$ cm$^6$ s$^2$ for the three-photon cross section and $10^5$ V/cm for the velocity term. For an absolute comparison of deposited energies, the scale in Fig. 17 has to be multiplied by a factor of 2 in this case. The important aspect of this qualitative result lies in the fact that field-dependent recombination is necessary to reproduce the functional shape of the photoacoustic signal. The recombination rates used above are also consistent with the delay experiment mentioned. The high fields of the heat pulse prevent carrier recombination only if the two pulses overlap. We find that maximum heating occurs at a delay of about 50 ps, which is consistent with the experimental data. In this calculation we have ignored the attenuation of the laser pulse due to free-electron absorption. As can be seen from Fig. 17, this is not justified for the conditions used by Jones *et al.*[6] A more quantitative investigation would thus require that the laser attenuation be included.

We have not included the temperature variation during the laser pulses. This variation is expected to change all scattering rates (except the impact ionization rate) used in the Monte Carlo integration of the Boltzmann equation. Therefore, the energy transfer rate and the high-field electron-multiplication rates would become temperature dependent. We have previously studied the implications of the temperature change during a laser pulse on the breakdown process at 1 $\mu$m wavelength.[35] These calculations were based on the assumption that the change of the scattering rates can be predicted within first-order perturbation theory. Since the LO-phonon energies are large, the LO rates are not expected to change much. The largest change would be expected for acoustic-phonon-related rates because the phonon energies are low and their population changes strongly with temperature. Recently, direct measurements of the acoustic-phonon scattering rate have been performed.[36] Unexpectedly, these experiments show no appreciable temperature dependence of the acoustic rate when the temperature is raised from 300 to 1200 K. This is most likely due to strong quantum effects at high electron energies where the scattering rates are large. Since the acoustic rate is by far the dominant scattering mechanism at energies above 2 eV, we are confident that the neglect of the temperature change during a laser pulse yields more accurate results in $SiO_2$.

## V. CONCLUSIONS

We have demonstrated the use of a methodology for quantitative studies of single-shot, laser prebreakdown and breakdown phenomena at visible and near-infrared wavelength in wide-band-gap insulators. The dynamics of free electrons in the presence of the strong electric field of a laser pulse (or alternatively in the presence of a dense photon population) was formulated by a Monte Carlo integration of the Boltzmann transport equation. Using the Monte Carlo method, accurate values for the energy transfer rate from the laser field to the lattice by free electrons (free-electron heating) and for the electron-multiplication rate by impact ionization can be calculated in a self-consistent manner if the proper approach for the laser-field–free-electron interaction is chosen. At long wavelengths the standard classical approach, whereby the laser field is implemented as a sinusoidal electric field, should be used. At short wavelengths the electron-photon interactions must be treated quantum mechanically such as with second-order perturbation theory.

We calculated the electron-multiplication rate and the energy transfer rate in $SiO_2$ and we compared in detail the results of the two different methods for the modeling of the electron-photon interaction. This comparative study showed that the classical approach is valid at wavelengths of 2 $\mu$m and higher, while the quantum approach is reliable at wavelengths of 500 nm and below. The two methods give upper and lower bounds for the calculated quantities at intermediate wavelengths. At wavelengths above 2 $\mu$m the calculated quantities approach the values in the dc limit. This is expected because the momentum relaxation rate becomes larger than the laser frequency. At long wavelengths, the calculated values for the power transfer saturate at values of about 10 $\mu$W/electron. With decreasing wavelength, both impact ionization and free-electron heating become less efficient. The impact ionization threshold rapidly shifts to higher fields at submicrometer wavelengths. Since multiphoton absorption becomes more efficient as the wavelength becomes smaller (as fewer photons are required to bridge the band gap), multiphoton absorption will become the dominant mechanism for free-electron generation at submicrometer

wavelengths. We find that free-electron heating at these wavelengths is still efficient enough to allow for strong lattice heating and melting at laser intensities well below the impact ionization threshold.

We have used the various quantities calculated with the Monte Carlo method as input parameters to rate equations which describe the evolution of the free-electron density, the total-energy transfer from the laser field to the lattice, and the increase in lattice temperature during realistic laser pulses in $SiO_2$. These calculations allow a semiquantitative discussion of the two-pulse laser experiments at prebreakdown laser powers in $SiO_2$.[6] We confirm that multiphoton-generated free-carrier heating accounts for the prebreakdown lattice heating in the two-pulse experiment. Our calculations indicate that a complete description of prebreakdown lattice heating due to high-power lasers requires, in addition to the calculation of multiphoton-absorption cross sections, the inclusion of the electron-hole recombination. At strong dc electric fields, the Monte Carlo method has been successfully used for the latter purpose,[34] and it should be possible to extend our method in this respect.

## ACKNOWLEDGMENTS

The authors wish to acknowledge stimulating discussions with D. J. DiMaria, M. V. Fischetti, F. R. McFeely, and P. Kelly on this topic. We also thank P. Kelly for providing additional information on the laser experiments performed at Washington State University.

---

*Present address: Department of Electrical Engineering and Computer Science, University of Illinois at Chicago, Chicago, IL 60640.

[1]A. Molchanov, Sov. Phys. Solid State **12**, 749 (1970).
[2]P. M. Mednis and V. M. Fain, Zh. Eksp. Teor. Fiz. **62**, 812 (1972) [Sov. Phys.—JETP **35**, 429 (1972)].
[3]E. Yablonovitch and N. Bloembergen, Phys. Rev. Lett. **29**, 907 (1972).
[4]A. Epifanov, Zh. Eksp. Teor. Fiz. **67**, 1805 (1974) [Sov. Phys.—JETP **40**, 897 (1975)].
[5]L. H. Holway, Jr. and D. W. Fradin, J. Appl. Phys. **46**, 279 (1975).
[6]S. C. Jones, P. Braunlich, R. T. Casper, X. A. Shen, and P. Kelly, Opt. Eng. **28**, 1039 (1989).
[7]B. Gorshkov, A. Epifanov, and A. Manenkov, Zh. Eksp. Teor. Fiz. **76**, 617 (1979) [Sov. Phys.—JETP **49**, 309 (1979)].
[8]H. Y. Fan, W. Spitzer, and R. J. Collins, Phys. Rev. **101**, 566 (1956).
[9]H. C. Huang, S. Yee, and M. Soma, J. Appl. Phys. **67**, 2033 (1990).
[10]M. Sparks, D. L. Mills, R. Warren, T. Holstein, A. A. Maradudin, L. J. Sham, E. Loh, Jr., and D. F. King, Phys. Rev. B **24**, 3519 (1981).
[11]F. R. McFeely, E. Cartier, J. A. Yarmoff, and S. A. Joyce, Phys. Rev. B **42**, 5191 (1990).
[12]F. R. McFeely, E. Cartier, L. J. Terminello, A. Santoni, and M. V. Fischetti, Phys. Rev. Lett. **65**, 1937 (1990).
[13]E. Cartier and F. R. McFeely, Phys. Rev. B **44**, 10 689 (1991).
[14]T. N. Theis, D. J. DiMaria, J. R. Kirtley, and D. W. Dong, Phys. Rev. Lett. **52**, 1445 (1984).
[15]M. V. Fischetti, Phys. Rev. Lett. **53**, 1755 (1984).
[16]D. J. DiMaria, T. N. Theis, J. R. Kirtley, F. L. Pasavento, D. W. Dong, and S. D. Brorson, J. Appl. Phys. **57**, 1214 (1985).
[17]S. D. Brorson, D. J. DiMaria, M. V. Fischetti, F. L. Pasavento, P. M. Solomon, and D. W. Dong, J. Appl. Phys. **58**, 1302 (1985).
[18]J. O'Dwyer, J. Appl. Phys. **40**, 3887 (1969).
[19]K. K. Thornber and R. P. Feynman, Phys. Rev. B **15**, 4099 (1970).
[20]A. Halim, M. Shousha, D. L. Pulfrey, and L. Young, J. Appl. Phys. **43**, 15 (1972).
[21]W. T. Lynch, J. Appl. Phys. **43**, 3274 (1972).
[22]T. H. DiStefano and M. Shatzkes, Appl. Phys. Lett. **25**, 685 (1974).
[23]D. K. Ferry, J. Appl. Phys. **50**, 1422 (1979).
[24]M. V. Fischetti, D. J. DiMaria, S. D. Brorson, T. N. Theis, and J. R. Kirtley, Phys. Rev. B **31**, 8124 (1985).
[25]R. C. Hughes, Phys. Rev. Lett. **30**, 1333 (1973).
[26]B. K. Ridley, *Quantum Processes in Semiconductors* (Clarendon, Oxford, 1988).
[27]D. Arnold, E. Cartier, and D. J. DiMaria, Phys. Rev. B **45**, 1477 (1992).
[28]J. N. Bradford and S. Woolf, Radiat. Eff. Defects Solids **117**, 227 (1991).
[29]D. J. DiMaria, M. V. Fischetti, J. Batey, L. Dori, E. Tierney, and J. Stasiak, Phys. Rev. Lett. **57**, 3213 (1986).
[30]D. J. DiMaria, D. Arnold, and E. Cartier, Appl. Phys. Lett. **60**, 2118 (1992).
[31]W. Porod and D. K. Ferry, Phys. Rev. Lett. **54**, 1189 (1985).
[32]P. Kelly (private communication).
[33]R. T. Williams, P. H. Klein, and C. L. Marquardt, in *Laser-Induced Damage in Optical Materials,* edited by A. J. Glass and A. H. Guenther (U.S. GPO, Washington, D.C., 1978), p. 481.
[34]D. A. Buchanan, M. V. Fischetti, and D. J. DiMaria, Phys. Rev. B **43**, 1471 (1991).
[35]D. Arnold, E. Cartier, and M. V. Fischetti, in *Laser-Induced Damage in Optical Materials: 1990,* edited by H. E. Bennett, L. L. Chase, A. H. Guenther, B. E. Newnam, M. J. Soileau, and D. R. Wolters (SPIE, Bellingham, Washington, 1991), Vol. 1441, p. 473.
[36]E. Eklund, F. R. McFeely, and E. Cartier, Phys. Rev. Lett. **69**, 1407 (1992).